Heavy residue formation in 20 MeV/nucleon ^{197}Au-^{12}C and ^{197}Au-^{27}Al collisions

G. A. Souliotis,[1,*] K. Hanold,[2,†] W. Loveland,[1] I. Lhenry,[2,‡] D. J. Morrissey,[3] A. C. Veeck,[2,§] and G. J. Wozniak[2]

[1]*Department of Chemistry, Oregon State University, Corvallis, Oregon 97331*
[2]*Lawrence Berkeley Laboratory, University of California, Berkeley, California 94720*
[3]*National Superconducting Cyclotron Laboratory, Michigan State University, East Lansing, Michigan 48824*
(Received 5 November 1997)

The yields and velocity distributions of heavy residues and fission fragments from the reaction of 20 MeV/nucleon ^{197}Au with ^{12}C and ^{27}Al have been measured using the MSU A1200 fragment separator. The mass and isotopic distributions of the reaction products are generally consistent with previously measured radiochemical data. One observes, especially for the Au+Al reaction, the production of very neutron deficient nuclides, possibly including ''new'' nuclei. The heavy-residue velocity distributions can be resolved into components due to fusionlike collisions (incomplete fusion, $v_{res}/v_{cn} \simeq 0.8$) along with components due to more peripheral interactions. Fusionlike events were observed that lead to near- and trans-gold species. The observed mass and charge distributions of the fusionlike products, sorted by velocity, are compared with the results of simulations using PACE2 and GEMINI of the decay of the excited incomplete fusion products. The simulations, while reproducing the general features of the data, predict residue distributions that are too neutron deficient relative to the observed distributions. The observed yields of the trans-gold species are not predicted in the simulations. [S0556-2813(98)00106-X]

PACS number(s): 25.70.Mn, 25.70.Jj, 27.90.+b

I. INTRODUCTION

We have known for some time [1,2] that the relative yields of the heavy residues, i.e., the large remnants of the heavy member of an asymmetric reacting pair of nuclei, increased with increasing projectile energy for intermediate-energy collisions. For example, in ^{12}C+Au collisions, the yields of the heavy residues increased from 3% of the reaction cross section at 20 MeV/nucleon to 50% at 86 MeV/nucleon [1]. Thus an understanding of the processes that lead to the formation of these products is an important part of understanding the dynamics of intermediate-energy collisions.

Unfortunately, there are experimental difficulties in studying the formation of these nuclei in asymmetric reactions using ''normal'' kinematics. The energies of the residues are low (~ 15 keV/nucleon [1]) and the masses are large. Frequently experimental thresholds cause one to miss substantial portions ($>50\%$) of the product distributions [1].

One can overcome the problem of detecting low fragment energies by studying these asymmetric reactions in ''inverse kinematics,'' i.e., bombard a low mass nucleus with a large mass nucleus. This ''transformation of the rest frame'' does, however, create the problem that all the heavy reaction products have similar velocities. For example, in 20 MeV/nucleon ^{197}Au-^{12}C collisions, a 12% shift in velocity of the heavy reaction product corresponds to the entire range of linear momentum transfers, i.e., 0–100 %. The use of a high-resolution detector to observe the projectilelike fragments (PLFs) in inverse kinematics solves this problem.

Pioneering studies by Bazin *et al.* [3], Faure-Ramstein *et al.* [4], and Hanold *et al.* [5] have shown the feasibility of this approach in studying the heavy reaction products from Kr+X and Xe+X mass asymmetric collisions at intermediate energies. These workers were able to show the importance of incomplete fusion, deep inelastic, and quasielastic reactions in forming these products. However, certain questions remain unresolved in these works. In the limited number of cases where one could compare the isotopically resolved measurements to radiochemical data, there were substantial discrepancies [5]. Since most of our detailed knowledge about these residues has come from radiochemical measurements, these discrepancies raise the question of how well we understand heavy residue production in mass asymmetric collisions. In addition, there was no substantial fission of the Xe- or Kr-like products in these studies with medium mass projectiles. While this simplification might be seen as an advantage, one was not able to utilize the fission probe (which is sensitive to the initial primary product's spin) to gain insight into the reaction processes as well as not being able to study the fission-particle emission competition at high excitation energies with isotopically resolved residue data.

For these reasons, we undertook the study of the interaction of 20 MeV/nucleon ^{197}Au with ^{12}C, ^{27}Al, ^{44}Ti, ^{90}Zr, and ^{197}Au using inverse kinematics and a magnetic separator to study the reaction products. In this paper, we report on the study of the ^{197}Au+^{12}C, ^{27}Al reactions. Our work is a direct extension, using similar techniques, of the work of Hanold *et al.* [5].

---

*Present address: Institute of Nuclear Physics, NCSR ''Demokritos,'' Athens, Greece.

†Present address: Syagen Technology, 1411 Warner Ave., Tustin, CA 92780.

‡Present address: Institut de Physique Nucleaire, 91406 Orsay, France.

§Present address: McKinsey and Company, Inc., 301 Grant Street, Suite 2600, Pittsburgh, PA 15219-1414.

The specific questions to be addressed in this work are the following. (a) What are the detailed mass and charge distributions of the residues (and their higher moments) as a function of residue velocity? (b) Do the results of the inverse kinematical studies of residue formation agree with the radiochemical studies of the same phenomena? (c) What information about the primary reaction mechanisms and/or the deexcitation (by fission or particle emission) of the primary heavy residue can be obtained from these data and a comparison with predictions of current models for intermediate-energy collisions?

The paper is organized as follows. In Sec. II, a description of the experimental apparatus, the measurements, and the data analysis is given. In Sec. III yield distributions are presented and compared with radiochemical measurements. Also the velocity distributions and the velocity-sorted yield distributions are discussed. In Sec. IV, the results of the measurements are compared to modern models of the deexcitation of hot heavy nuclei. Finally, conclusions from the present study are summarized in Sec. V.

II. EXPERIMENTAL

A. Description of apparatus

This experiment is a direct extension of the work of Hanold *et al.* [5] (who studied the interaction of 26–50 MeV/nucleon ^{129}Xe with Be, C, and Al) to the interaction of 20 MeV/nucleon ^{197}Au with C and Al. Apart from certain developments (outlined below) needed to treat the heavier projectile, the experimental apparatus and methods are those of Hanold *et al.* [5]. The reader is referred to that work and previous descriptions [7] of the MSU A1200 fragment separator and its operation for a detailed description of the experimental apparatus.

The experiment was performed at the National Superconducting Cyclotron Laboratory at Michigan State University. A 20 MeV/nucleon ^{197}Au beam, produced by the K1200 cyclotron, interacted with ^{12}C and ^{27}Al targets of thickness 1.0 and 2.0 mg/cm^2, respectively. (The target thicknesses were such that the maximum energy loss of the beam in traversing the target was 0.46 and 0.74 MeV/nucleon [6].) The reaction products were analyzed using the A1200 fragment separator [7]. The A1200 was operated in a medium acceptance mode [with an angular acceptance of 0.8 msr ($\Delta\theta = 20$ mr, $\Delta\phi = 40$ mr) and a momentum acceptance of 3%]. The primary beam struck the target at an angle of 0.8° relative to the optical axis of the spectrometer. In the medium acceptance mode, the A1200 has two intermediate dispersive images and a final achromatic image (focal plane). At the focal plane, the fragments were collected in a three-element (ΔE_1, ΔE_2, E) Si surface barrier detector telescope. The 300 mm^2 Si detectors were 50, 50, and 400 μm thick, respectively. A schematic diagram of the spectrometer and the detector arrangement is shown in Fig. 1.

Time of flight was measured between two plastic scintillators of thicknesses 0.25 and 1.25 mg/cm^2 positioned at the first dispersive image and at the focal plane, respectively, and separated by a distance of 14 m. An $X-Y$ position sensitive parallel-plate avalanche counter (PPAC) was used at the first dispersive image to record the position of the reaction products. The horizontal position, along with NMR
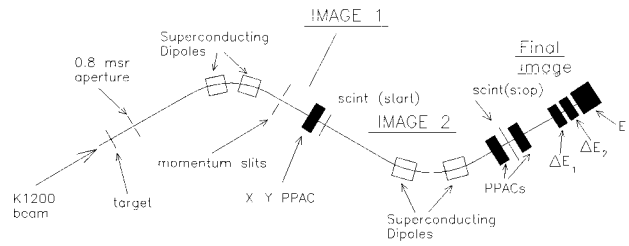

FIG. 1. Schematic diagram of the A1200 spectrometer and the detector arrangement used in the study of ^{197}Au-induced reactions at 20 MeV/nucleon.

measurements of the A1200 dipole fields, was used to determine the magnetic rigidity $B\rho$ of the particles. Thus the reaction products were characterized by an event-by-event measurement of dE/dx, E, time of flight, and magnetic rigidity.

To cover a large range of fragments and their momentum distributions, a series of measurements at overlapping magnetic rigidity settings of the spectrometer was performed. Normalization of beam current for data taken at different settings was obtained with a set of four monitor detectors mounted around the target position.

B. Calibration procedures and data analysis

The relation between the magnetic rigidity and the horizontal position at the first dispersive image was calibrated by observing the position of the primary beam in various charge states as a function of the magnetic rigidity settings of the spectrometer. The magnetic rigidity resolution [full width at half maximum (FWHM)] was better than 0.1%. The time-of-flight measurement with the scintillators resulted in a velocity resolution of about 0.8%.

The Si detector telescope was calibrated with a low intensity ^{197}Au primary beam and a series of analog beams (^{129}Xe, ^{95}Mo, ^{54}Fe, ^{54}Cr, and ^{27}Al) at 20 MeV/nucleon and also, with degraded scattered ^{197}Au particles (in various charge states, present at several settings of the A1200) which provided a calibration of the response of the Si detectors to 14–20 MeV/nucleon ^{197}Au ions. The energy loss in each of the two transmission detectors (ΔE_1 and ΔE_2) was calculated [6] and, knowing the initial energy, the energy deposited in the stopping (E) detector was calculated.

The transmission detectors were calibrated by directly correlating pulse height with energy loss using simple polynomial functions. This calibration was adequate for the energy loss reconstruction of most of the events of interest (see the Appendix). For the stopping (E) detector, pulse-height defect (PHD) corrections were necessary to obtain an accurate reconstruction of the residual energy of the particles. For this purpose, we developed a simple procedure, based on Moulton's formulation [8] and the calibration beam data, which is outlined in the Appendix. The measurement of the total energy E_{tot} of the particles entering the spectrometer (obtained from the sum of the energies deposited in the Si detectors plus small corrections due to the presence of the scintillators and the PPACs) had an overall resolution (FWHM) of approximately 2%.

The determination of the atomic number Z was based on the measurement of the energy loss of the particles in the first transmission detector and their velocity. From Bethe's stopping power formula, the atomic number of an ion entering a given material at a given velocity can be expressed as

$$Z \propto v \sqrt{\Delta E}, \tag{1}$$

where v is the velocity of the ion entering the detector and ΔE the energy loss. Guided by Eq. (1), we empirically expressed Z as a quadratic function of the product $v\sqrt{\Delta E}$ with velocity-dependent coefficients

$$Z = a_0(v) + a_1(v) \, v\sqrt{\Delta E} + a_2(v)(v\sqrt{\Delta E})^2. \tag{2}$$

In order to determine the functions $a_0(v)$, $a_1(v)$, and $a_2(v)$ in the velocity range of interest, we used the data of Hubert *et al.* [6] to obtain the coefficients of Eq. (2) for the Z range 30–90 and in the energy range 12–24 MeV/nucleon by applying a least-squares fitting procedure at each energy, in steps of 1 MeV/nucleon. Subsequently, the values of each coefficient at the various energies were fitted with polynomial functions of velocity. The atomic number Z of the particles was reconstructed from the measured ΔE and v using Eq. (2) with a resulting resolution (FWHM) of 0.9 Z units for heavy residues and 0.6 Z units for fission fragments.

The ionic charge q of the particles entering the A1200 was obtained from the total energy E_{tot}, the initial velocity and the magnetic rigidity according to the expression

$$q = \frac{3.107}{931.5} \frac{E_{\text{tot}}}{B\rho(\gamma - 1)} \beta\gamma, \tag{3}$$

where E_{tot} is in MeV, $B\rho$ in Tm, $\beta = v/c$, and $\gamma = 1/(1 - \beta^2)^{1/2}$. The measurement of the ionic charge q had a resolution of 0.9 q units for heavy residues and 0.6 q units for fission fragments. Since the ionic charge must be an integer, we assigned integer values of q for each event by putting windows ($\Delta q = 1$) on each peak of the q spectrum. Using these integer q values, along with the magnetic rigidity and velocity measurements, the mass A of each ion was obtained from the expression

$$A = q \, \frac{B\rho}{3.107\beta\gamma} \tag{4}$$

with an overall resolution (FWHM) of about 1.5 A units for heavy residues and 1.1 A units for fission fragments. (It should be noted that this resolution is much better than the resolution obtained by calculating the mass A using E_{tot} and velocity directly, since E_{tot} alone has a resolution of 2.0%.)

From the values of Z, q, A, and v determined on an event-by-event basis, the procedure outlined below was applied to the data in order to extract physically interesting distributions of the reaction products. For each data set at a given magnetic rigidity, bins of width 1 Z unit were set on the Z spectrum and for each Z bin, the corresponding q spectrum was obtained. For each Z bin and for every q bin of this Z, a two-dimensional histogram of the yield with respect to $B\rho$ and velocity was constructed.

It should be noted that for a given element Z with initial velocity v, the presence of the scintillator and the PPAC at

the first dispersive image of the A1200 creates an equilibrium charge distribution for each ionic charge q that has been selected by the first pair of dipoles. Since the rigidity of the second pair of dipoles was not scanned for each setting of the first pair, only a part of this distribution was accepted by the detector telescope at the focal plane. Specifically, the aperture of the detector and the dispersion of the spectrometer were such that only one charge state of this distribution could be accepted. In order to account for the missing part of this distribution, a correction factor was applied to the yield of each bin of the $B\rho$ vs velocity histogram (of every Z and q bin). The equilibrium charge distribution for given Z and velocity was calculated according to Baron *et al.* [9]. The resulting correction factors were on average about 4 for heavy products and smaller (2–3) for medium mass products. Subsequently, for every Z and q window, the $B\rho$ vs velocity histogram was converted into an A vs velocity histogram and properly normalized and combined for each magnetic rigidity setting, resulting in a distribution in Z, q, A, and velocity. Finally, after integration over the ionic charge q, a distribution of the yield with respect to Z, A, and velocity was generated for each of the reactions studied.

The resolutions achieved in these measurements of ^{197}Au fragmentation with respect to Z, A, q, and velocity (FWHM $= 0.9$, 1.5, 0.9, 0.8 %, respectively) are poorer than those obtained by Hanold *et al.* [5] for studies of ^{129}Xe at higher energies (FWHM $= 0.36, 0.35, 0.28, 0.5$ %). The lower resolution is due to the poorer time resolution in this experiment, and to problems (poorer energy resolution) associated with the detection of the Au-like fragments, as compared to the Xe-like fragments. Also we wish to note that while all Si detectors were operated at voltages that guaranteed depletion, they could not be operated at their recommended operating voltages because, at that voltage, they would undergo an apparent "avalanching" discharge in response to Au-like fragments. The operating voltages had to be reduced to prevent this phenomenon.

The observed yield distribution must be corrected for the limited angular acceptance of the spectrometer to provide absolute production cross sections. Hanold *et al.* [5] made this correction using an incomplete fusion-evaporation model calculation. We used the measured angular distributions [10] of the heavy residues from the similar reaction of 20 MeV/nucleon ^{129}Xe with ^{12}C and ^{27}Al to make the correction. Elemental cross sections of heavy residues with $Z = 42$–57 were obtained by integrating the angular distribution of each element. Correction factors for the limited A1200 angular acceptance were determined for each element from the fraction of its cross section that fell into the spectrometer angular acceptance. To use these correction factors for the heavy residues produced in the present Au-induced reactions, we assumed that the heavy residue angular distributions do not change appreciably with the change of the projectile from ^{129}Xe to ^{197}Au and scaled the residue masses relative to the corresponding projectile mass. The mass-dependent correction factors for the absolute values of the heavy residue yields range from 1–2 for ^{197}Au + ^{12}C and 1–7 for ^{197}Au + ^{27}Al. The fission fragment yield correction factors were determined with a model calculation similar to that used in Ref. [5].

Because of well-known difficulties in measuring the absolute beam intensities and correcting for transmission losses in the A1200 spectrometer [5,11] (leading to uncertainties of factors of 2–100 in the absolute cross sections) we normalized our measured nuclidic production cross sections for the 20 MeV/nucleon ^{197}Au+^{12}C reaction to the known production cross sections determined in a threshold-free radiochemical study [12] of the 20 MeV/nucleon ^{12}C+^{197}Au reaction. We did this using the ratio of the nonisomeric, independent yield production cross sections measured by Kudo *et al.* [12] to the values measured in this work for the same nuclides. We have assumed the same normalization factor for all products formed in the ^{197}Au+^{27}Al reaction. This normalization factor has a value of 7 which is consistent with previous work [5] in which large discrepancies between the absolute cross sections deduced from A1200 measurements and other work was found.

III. RESULTS AND DISCUSSION

A. Cross sections

Velocity integrated yield distributions for the two reactions studied in this work are shown as Z,A contour plots in Fig. 2. The Z coordinate is given relative to the line of beta-stability Z_β which was taken as $Z_\beta = (113.029 - 132.89A^{-1/3})/2(0.717A^{-1/3} + 111.036A^{-1} - 132.89A^{-4/3})$ [13]. The centroids of the fission and residue distributions lie on the neutron-deficient side of stability. Because complete scans of the spectrometer were not done for the fission fragments, the light fission fragment distributions are not available. In the Au+C reaction, the residue distributions are narrow and well separated from the fission fragment distributions while in the Au+Al reaction, the residue distribution is broader. There is satisfactory agreement between the locus of the most probable primary fragment atomic number Z_{mp} determined in previous radiochemical studies of similar reactions [12,2] (indicated by straight line segments in Fig. 2) and the centroids of the yield contours. In the Au+C system, the Z distribution at constant A shows two peaks near $A \sim 200$, corresponding (see below) to fusionlike and peripheral collisions, a feature noted previously [12].

In Fig. 3, we show the isobaric yield distributions for the two reactions along with the results of radiochemical studies [12,2] of similar reactions. The agreement between the shapes of the two measured mass distributions for the C+Au reaction is fair. The yields of fragments close to ^{197}Au are lower (by a factor of 5) in the A1200 data compared to the radiochemical data, due to the loss of quasielastic products (in the spectrometer data) which cannot be magnetically separated from elastically scattered ^{197}Au nuclei. The spectrometer data indicate higher yields of the trans-gold species than observed in the radiochemical data. Detailed numerical simulations with the measured resolution functions show this effect is not due to the poorer resolution of the spectrometer measurements. Similarly, the large discrepancies in yields at $A = 170–180$ or $A = 125–145$ for Au+C appear to be real and not the effect of resolution. One can say there is general qualitative agreement between the mass yield curves measured by the two techniques, but serious discrepancies exist in a quantitative comparison, which are only partly explained by the limitations of the A1200 spectrometer.
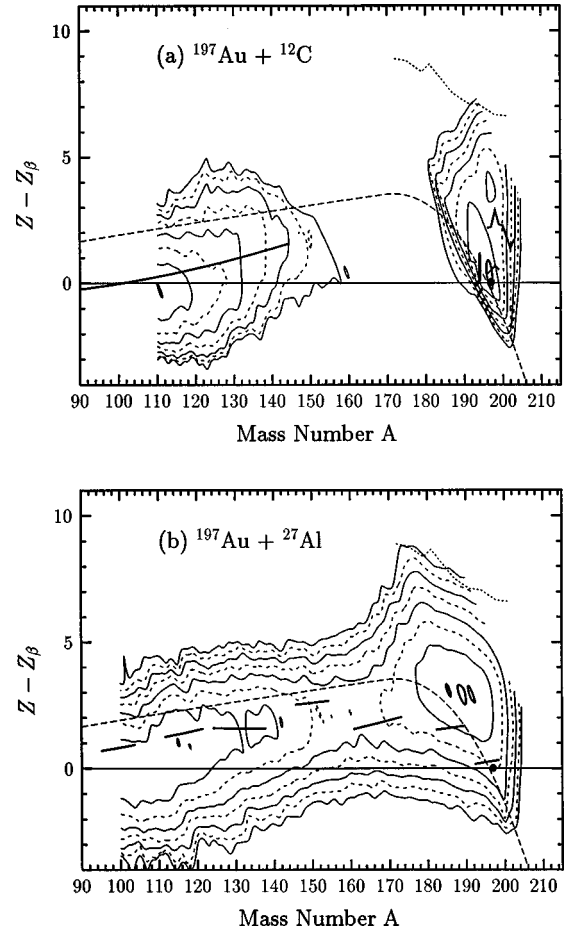

FIG. 2. (a) Yield of fragments from the 20 MeV/nucleon ^{197}Au+^{12}C reaction as a function of Z (relative to the line of beta stability Z_β) and A. (b) same as (a) except the reaction is 20 MeV/nucleon ^{197}Au+^{27}Al. The short line segments in each plot represent the most probable primary fragment Z values as determined in radiochemical studies of similar reactions [12,2]. The dashed line indicates the expected Z_p for relativistic nuclear collisions [16]. The dotted line indicates the A values of the lightest known nucleus for each Z.

The product mass distributions for the Au+C and Au+Al reactions appear to differ significantly. Qualitatively, this difference might be expected to be due, in part, to the higher excitation energy and the more fissionable nature of the composite species formed in the reaction with the Al target. However, we will show below that there are differences in reaction mechanisms between these two systems. This difference in apparent reaction mechanisms (as reflected in the mass distributions) agrees with previous observations of the reaction of 26 and 34 MeV/nucleon Kr with C and Al [4] and the reaction of 24 MeV/nucleon ^{238}U with C and Si [14], but disagrees with observations [5] of the interaction of 26 MeV/nucleon ^{129}Xe with C and Al where little difference was observed between using C or Al target nuclei. Comparison of these data (Fig. 3) with the mass yield curve for the interaction of 16 MeV/nucleon ^{32}S with ^{197}Au [2] shows the gross overall agreement in the comparisons between the radiochemical and spectrometer data. Of particular note in the Au+Al mass distribution is the fact that the maximum yield of the goldlike fragments occurs at $A \sim 187$, a shift of ~ 10 A units from the mass number of the gold nucleus.
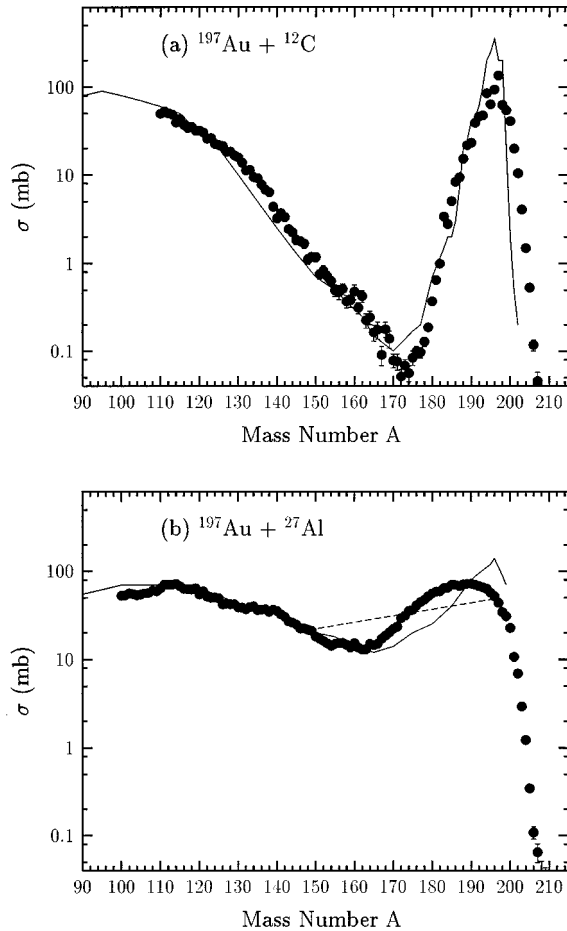
FIG. 3. The isobaric yield distributions for the reaction systems shown in Fig. 2. The solid and dashed curves refer to the radiochemical data cited in Fig. 2.

FIG. 4. Typical heavy residue charge distributions for the interaction of 20 MeV/nucleon ^{197}Au with ^{12}C. The dashed curves and open circles show the radiochemical data [12] for the inverse reaction.

This shift is not seen in studies of similar reactions at lower and higher energies and would, if confirmed in a measurement that was more sensitive to quasielastic events, represent an unusual drift or mass flow in the reaction.

In Fig. 4, we show the isobaric charge distributions for Au+C reaction, while in Fig. 5 we show similar data for the Au+Al reaction. Also shown in Fig. 4, are the data for the radiochemical study of the C+Au reaction. One notes the rather complete character of the charge distributions with up to 12 points spanning two or more orders of magnitude per A value compared to the 2–4 points typically measured in a radiochemical experiment. The charge distributions for the trans-gold products are double humped for the Au+C reaction, and (see below) reflect contributions from peripheral collisions ($Z \sim 79$) and fusionlike collisions ($Z \sim 82$–83). In comparing the spectrometer and radiochemical measurements, we have not considered regions ($A = 195$–198) where the spectrometer resolution is inadequate to separate beam and quasielastic events or radiochemical data that does not represent an ''independent yield,'' i.e., has no contribution from β-decay feeding. The agreement between the spectrometer measurements and the radiochemical data is consistent with previous comparisons [15] between radiochemical and mass spectrometric measurements, apart from the previously noted discrepancies in the yields of the trans-gold products.
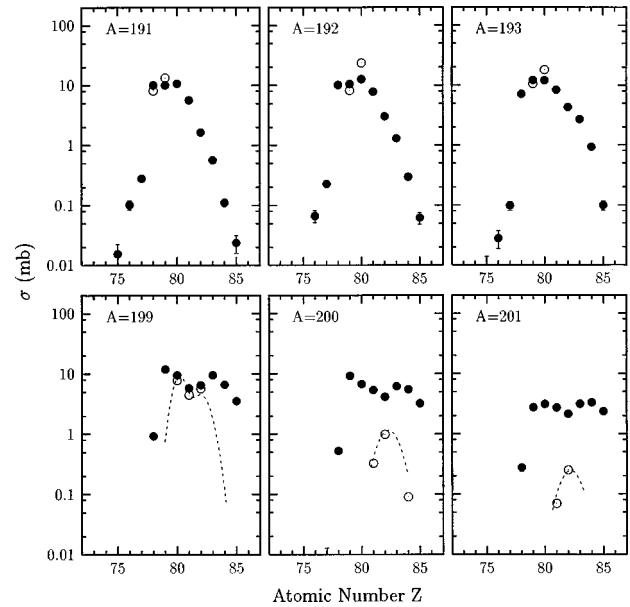
The charge distributions from the Au+Al reaction show similar trends to those noted for the Au+C reaction. The widths of the Au+Al distributions are, in general, broader than those from the Au+C reaction. For both the Au+C and Au+Al reactions, the shapes of the measured charge distributions are Gaussian, vindicating a frequent but unverified assumption in radiochemical studies.

In Figs. 2, 3, and 5, we show (as dashed lines) the expected most probable fragment atomic number, isobaric yield distribution and charge distributions based on the systematics for the interaction of relativistic protons and heavy ions [16] for the Au+Al reaction. This parametrization of Summerer et al. [16] does not describe the data of this work adequately, as might be expected, since it is an empirical compilation of data for higher energy reactions. The predicted Z_p from the Summerer formulation is 1–2 Z units too n-rich for a given A compared to the centroids of the observed distributions (Fig. 2) and the mass yield curve does not show a simple exponential decrease from the target mass number to lower mass numbers. It is also interesting to note the broader charge distributions observed in this work compared to the Summerer formulation [16]. The differences are larger than one would expect on the basis of the spectrometer resolution. They would suggest the fragmentation of heavy nuclei at intermediate energies may be a more effective way to make n-deficient nuclei than nucleon- or nucleus-induced spallation reactions. This observation may be of importance for new radioactive beam facilities.

In summary, there is fair agreement between previous radiochemical measurements of the overall cross sections and the present measurements. Some puzzling discrepancies (the trans-gold yields) exist. The spectrometer measurements and traditional radiochemical measurements are complementary with more detailed information such as the fragment velocities, being available in the spectrometer measurements, but the radiochemical measurements are threshold-free and
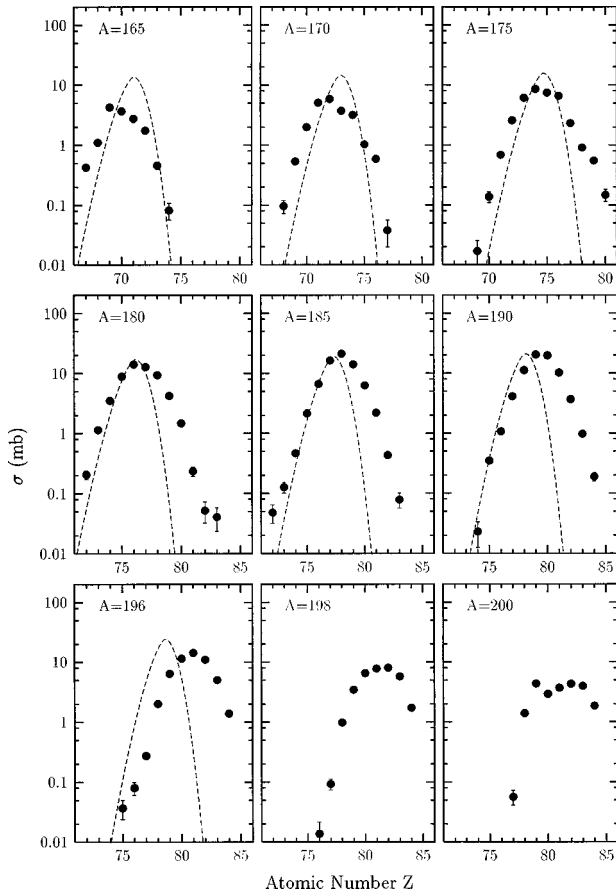
FIG. 5. Typical heavy residue charge distributions for the interaction of 20 MeV/nucleon ^{197}Au with ^{27}Al. The dashed curves show the expected charge distributions for relativistic nuclear collisions [16].

sample the entire reaction rather than fragments being emitted within the limited solid angle of the spectrometer.

B. Velocity distributions—heavy residues

In Fig. 6, we show the invariant velocity spectra for all detected products for the two reactions studied. Three peaks are observed in the Au+C distribution. One peak (near the velocity of the ^{197}Au projectile) corresponds to peripheral collisions while the second peak (with a velocity near that of the completely fused system) corresponds to fusionlike collisions. The third peak occurs at a velocity corresponding to the addition of the momenta of half of the residue following incomplete fusion and the average momentum of a symmetric fission fragment. With some imagination, the same three peaks can be found in the Au+Al velocity distributions. [To make a clear connection between features of the heavy residue distributions in inverse kinematics with those observed in normal kinematics of asymmetric collisions, we note that, in inverse kinematics, complete fusion corresponds to a minimum velocity of the composite system, whereas incomplete fusion and deep-inelastic/quasielastic collisions correspond to progressively higher velocities (but, of course, lower than that of the projectile velocity). We also note that, the evaporation of nucleons or light particles from an excited nucleus is isotropic in the rest frame of the nucleus, thus resulting in a broadening of the observed velocity distribu-
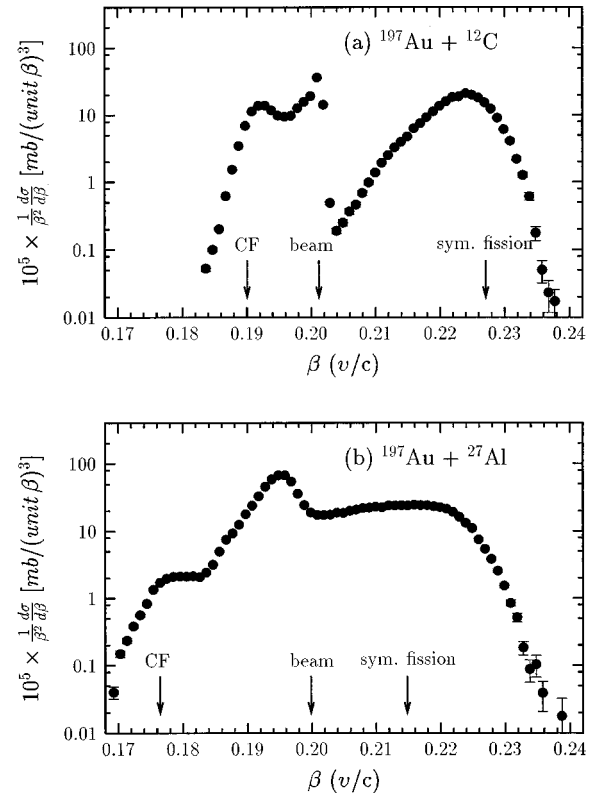

FIG. 6. Invariant velocity spectra for all detected products for the interaction of 20 MeV/nucleon ^{197}Au with (a) ^{12}C and (b) ^{27}Al. The velocities corresponding to complete fusion, the projectile and 80 percent momentum transfer followed by symmetric fission are shown by arrows.

tions, without affecting their mean values. Consequently, the average velocity of the observed heavy residues reflects the velocity of the excited nuclei formed in the primary interaction stage.]

To better resolve the various components of the velocity spectra, we show (Fig. 7) the mass resolved velocity distributions as contour plots. The fission, incomplete fusion and peripheral events are now clearly resolved for both reactions. In the detailed expansion of the residue distributions shown in Fig. 8, we note that the fractional linear momentum transfer (FLMT) for the fusionlike events is 0.80 and 0.83 for the Au+C and Au+Al reactions, respectively. These FLMT values are consistent with the systematics of linear momentum transfer [17] and observations for similar reactions [18]. We note that the FLMT values are also consistent with pre-equilibrium calculations [19] for these reactions which give values of the FLMT of 0.82 and 0.80 for the Au+C and Au+Al reactions. This agreement encourages us to think the mean number of pre-equilibrium particles agrees with predictions. These predictions suggest an average pre-equilibrium emission of 1.8 neutrons and 0.4 protons for the Au+C reaction and 4.7 neutrons and 1.0 protons for the Au+Al reaction.

Given the small, estimated number of pre-equilibrium particles, we have estimated the properties of the primary incomplete fusion (and peripheral collision products) by assuming binary kinematics as

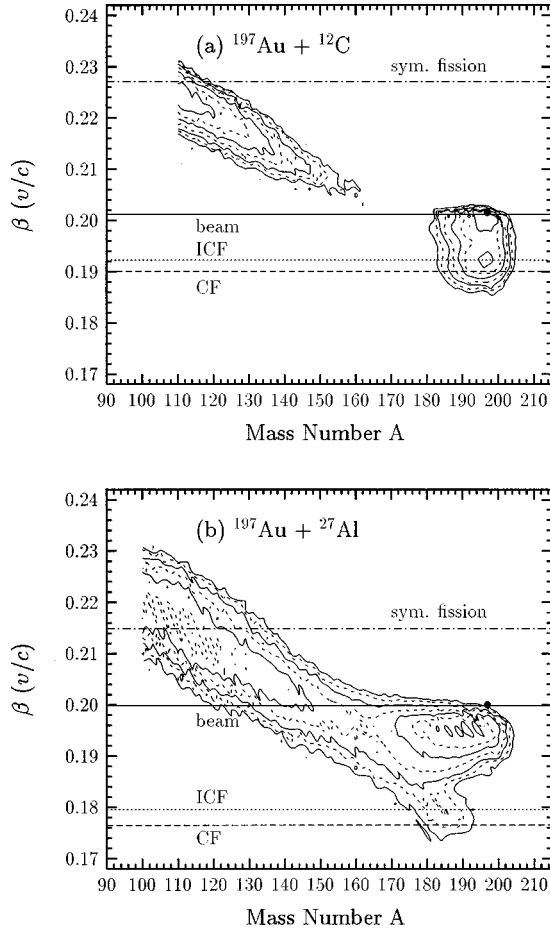$$Z_{ICF} = Z_{proj} V_{proj} / V_{ICF}, \qquad (5)$$

FIG. 7. The mass-resolved velocity distributions for the reactions studied in this work. The definitions of the velocity markers are the same as in Fig. 6 except a line (ICF) corresponding to 80% momentum transfer has been added.

$$A_{\text{ICF}} = A_{\text{proj}} V_{\text{proj}} / V_{\text{ICF}}, \qquad (6)$$

$$E^*_{\text{ICF}} = E^*_{\text{CF}} (V_{\text{proj}} - V_{\text{ICF}}) / (V_{\text{proj}} - V_{\text{CF}}), \qquad (7)$$

where Z_{ICF}, A_{ICF}, and E^*_{CF} refer to the average Z, A, and excitation energy of the primary residue following incomplete fusion. For complete fusion, $E^*_{\text{CF}} = 208$ and 401 MeV for the Au+C and Au+Al reactions. The ''average'' primary product nuclei following incomplete fusion are $^{207}_{84}$Po($E^*_{\text{ICF}} = 188.4$ MeV, $T = 3.2$ MeV) and $^{219}_{90}$Th ($E^*_{\text{ICF}} = 345$ MeV, $T = 4.2$ MeV) for the two reactions. One can integrate the yield contours in Fig. 7 to get estimates of the cross section for residue production in *fusionlike events*. These cross sections are 300 and 80 mb, respectively, for the Au+C and Au+Al systems. The former value for the fusionlike residue cross section is similar to that found (300 mb) for the reaction of 35 MeV/nucleon N+Au [20]. These authors found $\sigma_{\text{fission}} \simeq 1420$ mb which agrees with the measured value of 1700 mb for the C+Au reaction [12] and the estimate of σ_{fission} (1500 mb) made by doubling the number of fission events seen in our data. If we assume the estimated fission cross section (1500 mb) is due primarily to fusionlike events, we find for the Au+C reaction, a total cross section for fusionlike events of 1800 mb. This estimate is consistent with previous work [20,21]. Since Wile *et al.* [22] have mea-
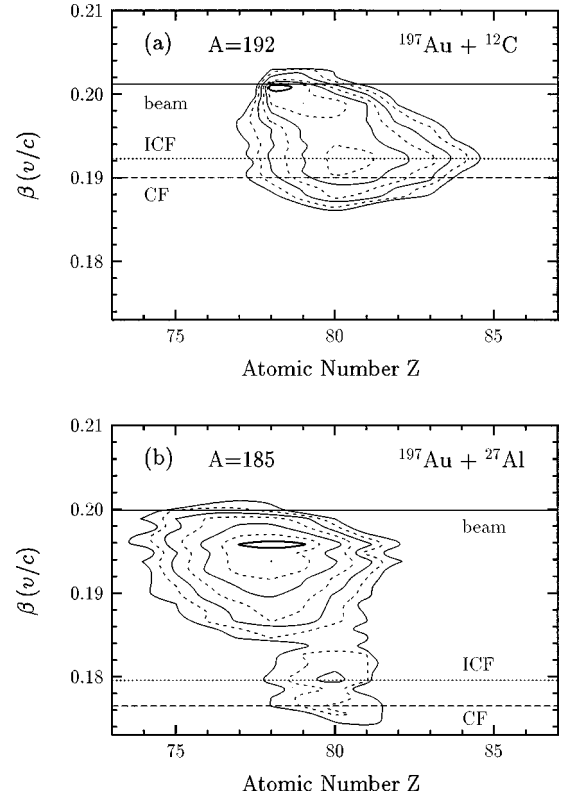

FIG. 8. Typical (Z,A) resolved velocity distributions for heavy residues.

sured the cross section for intermediate mass fragment (IMF) emission in the reaction of 20 MeV/nucleon ^{14}N+^{197}Au to be 127 mb, a value similar to the fusionlike residue cross sections, we conclude that a proper description of residue production must include IMF formation [23]. If one assumes a $2J+1$ distribution of J values leading to residue formation, these fusionlike residue cross sections can be used to estimate the spins and their dispersions for the precursors of the residues. The mean J values deduced in this way are similar ($23\hbar$ and $24\hbar$) for the precursors of the residues from fusionlike events for the Au+C and Au+Al reactions. These estimates of the properties of the primary nonfissioning residue populations can be used (Sec. IV) in comparisons with models of these collisions.

One additional feature of the A-resolved velocity distributions (such as Figs. 7 and 8) worthy of note is that the residue mass number is not a good impact parameter trigger, as it is in higher-energy collisions. One can observe, for a given mass number, a range of residue velocities (transferred momenta) which indicate a range of impact parameters. This feature is consistent with Boltzmann-Uehling-Uhlenbeck (BUU) calculations [24] of residue properties in similar systems at somewhat higher energies.

One can gain further insight into the impact parameter dependence of residue formation using the residue velocities to sort the data. To define a velocity scale that can be related to impact parameter in a simple way, the velocities of the residues were transformed in the moving frame of the projectile and were expressed as a fraction of the complete-fusion velocity (in the projectile frame). (In this definition of fractional velocity v_R / v_{CF}, commonly used in normal kinematics, complete fusion corresponds to $v_R / v_{\text{CF}} \simeq 1$, and peripheral collisions to $v_R / v_{\text{CF}} \simeq 0$.)
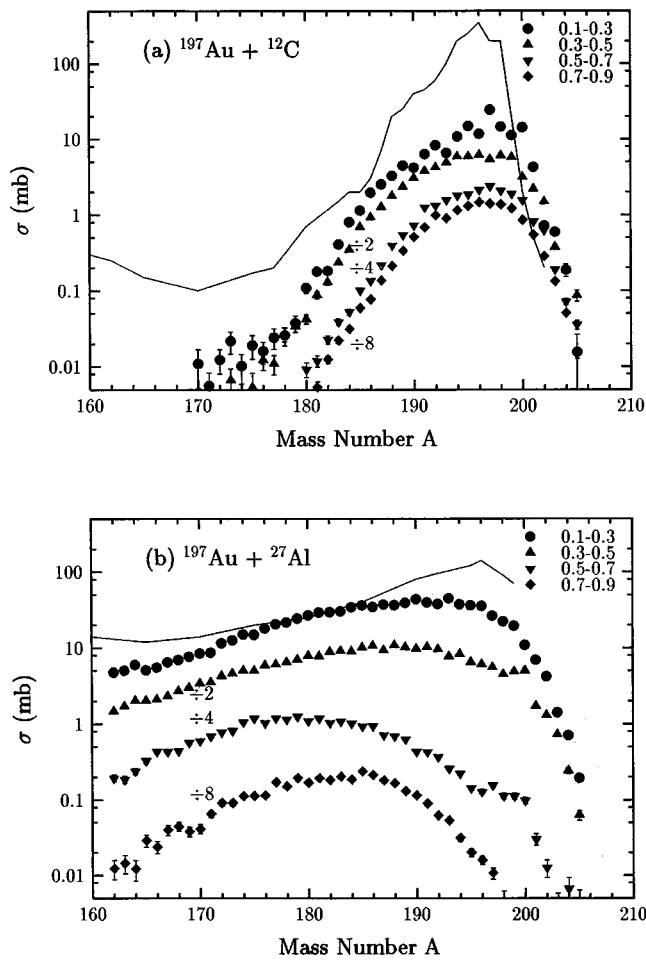
FIG. 9. Heavy residue isobaric yield distributions sorted by residue velocity v_R expressed as v_R/v_{CF}. The curves are displaced for viewing. The solid line shows the overall radiochemical mass distribution [12,2].

FIG. 10. Centroids of the heavy residue charge distributions sorted by residue velocity. Solid lines show the data from Refs. [12,2].

The two-dimensional Z vs A distributions of the heavy residues were generated for five velocity intervals spanning the range of v_R/v_{CF} from 0.0 to 1.0. Subsequently, for each velocity interval, the isobaric yield distributions [Figs. 9(a) and 9(b)] were created. From the isobaric Z distributions of the residues, the centroids and standard deviations were obtained (Figs. 10 and 11). A cursory examination of the data shown in Figs. 9–11 shows expected trends. As the transferred momentum increases, the excitation energy of the primary residues increases, leading to neutron emission that produces residues that are more neutron deficient. The widths of the secondary residue charge distributions also generally increase with increasing excitation energy of the residue precursor. Where comparisons are possible for the Au+C reaction, the radiochemical measurements [12] appear to be in acceptable agreement with this work although the assignment of events as fusionlike or quasielastic in that work was arbitrary.

A very interesting feature of the fusionlike products $(v_R/v_{CF} \sim 0.80)$ is the presence of heavy residues very close in charge and mass to the compound nucleus ^{209}At $(E^* \simeq 208$ MeV) (Figs. 9 and 10). These products have appreciable yields and are not due to tails of the yields of lower mass residues due to the resolution of the spectrometer. Similar
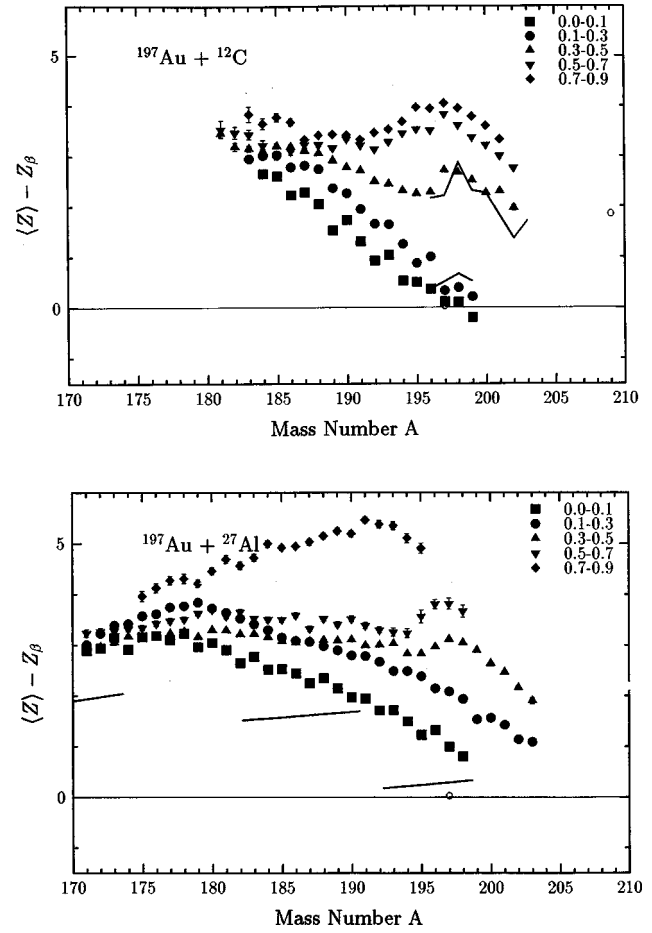
products have been observed in a recent radiochemical study of the reaction of 10 MeV/nucleon C+Au and were satisfactorily described by means of a Boltzmann master equation approach [25]. A satisfactory accounting for these events (Sec. IV) represents a stringent test for models of residue production. Also, as shown in Fig. 9 and observed previously [12], quasielastic processes are the primary source of the trans-gold species.

What is also remarkable about the data shown in Figs. 10 and 11 (especially for the Au+Al reaction) is the large widths of the charge distributions $(\sigma=1.5)$ combined with the very neutron-deficient centroids $(Z-Z_p=3-5)$ of the charge distributions. In Fig. 2, we show the locations of the lightest known nuclei for each Z. (Many of these nuclei are known to be short-lived proton emitters.) While the resolution of our measurements is not sufficient to establish the production of several "new" nuclei, the data do suggest that intermediate-energy reactions, such as those studied in this work, could be important paths to the production of heavy, nonspherical proton-rich nuclei and thus enable the study of barrier penetration and shell structure in heavy, deformed systems. Specifically, one notes (Fig. 5) the production of species such as the known proton emitter [26] ^{185}Bi with a cross section of 80 μb compared to that measured for the ^{95}Mo(^{92}Mo,pn)^{185}Bi reaction of 0.1 μb. This suggests that intermediate-energy reactions, such as those studied in this
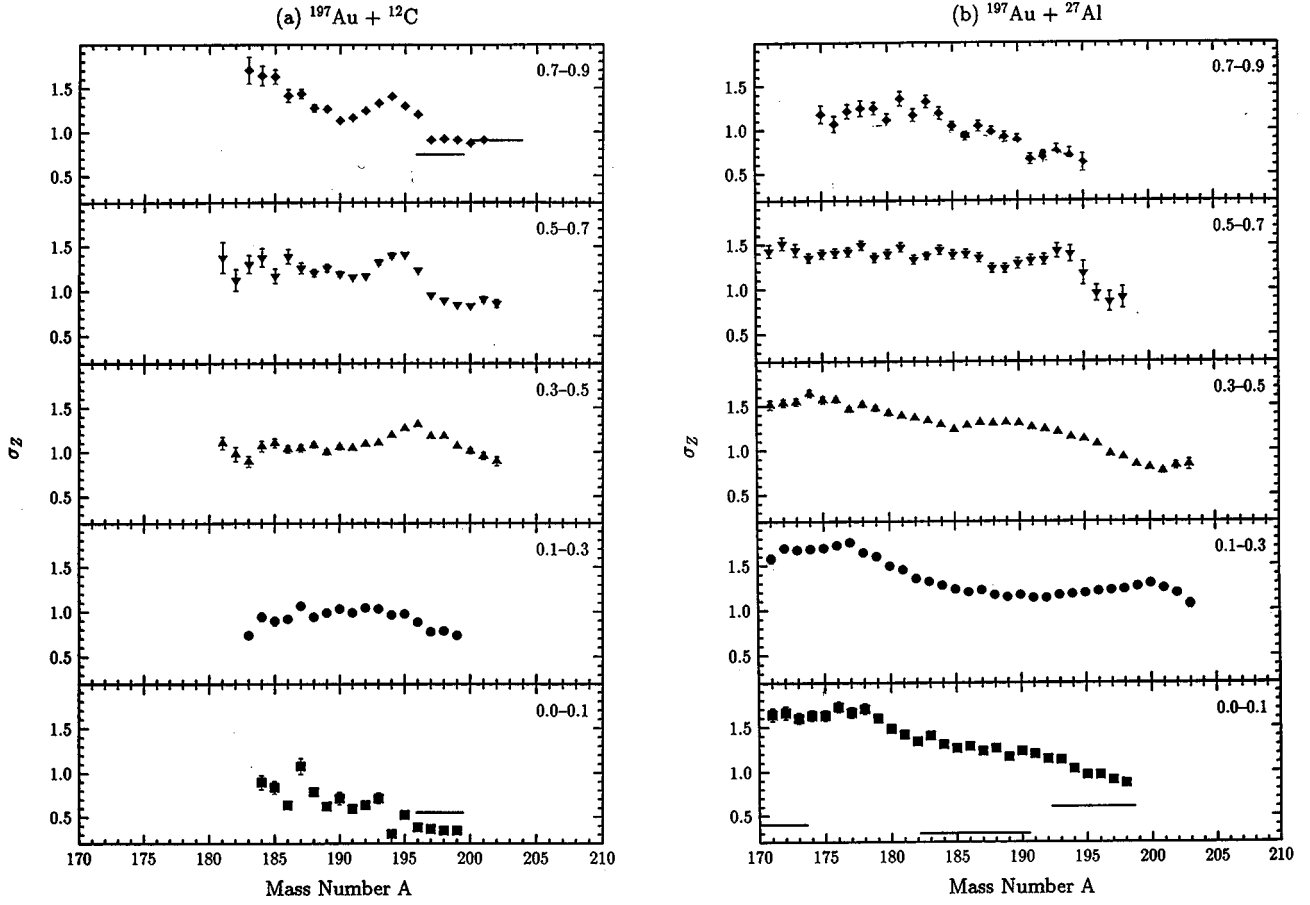
FIG. 11. The dependence of the Gaussian width parameter σ upon residue velocity and mass number. The solid lines indicate the data from Refs. [12,2].

work, with their unusually large residue survival probabilities, may be viable alternatives to the traditional compound nuclear reactions for producing p-rich nuclei.

Comparison of the velocity-resolved data from the Au+C and Au+Al reactions shows a number of differences between the two reactions. In the Au+Al reaction, as the transferred momentum (residue velocity) increases, the average mass number of the surviving residue shifts to lower values while in the Au+C reaction, the average residue mass is relatively insensitive to the transferred linear momentum. The widths of the charge distributions are generally larger for most velocity bins for the Au+Al reaction compared to the Au+C reaction, except for the fusionlike collision bin ($v_R/v_{CF} \sim 0.7-0.9$) where the reverse is true.

The dependence of the charge distribution widths upon residue mass number shows some significant peaks ($A \sim 194$ for Au+C, etc.). A careful examination of the data shows each of these "peaks" to be associated with a sharp change in the mean fragment atomic number (vs A), indicating, we believe, a change in the primary residue formation mechanism.

C. Fission fragment distributions

As indicated above, an incomplete scan of the fission fragment distributions was made. However, it is interesting to see what we might learn from studying the heavy fragment distributions we have. The first question that we might pose is whether we can understand what the average fissioning system was for the Au+C and Au+Al reactions. Information regarding this issue can be found in a plot of the average fragment velocities vs the fragment mass number (Fig. 12). If we assume massive transfer and the validity of a simple pocket formula for fission fragment kinetic energies, i.e.,

$$TKE = \frac{Z_1 Z_2 e^2}{1.8(A_1^{1/3} + A_2^{1/3})} \qquad (8)$$

we can, using an iterative procedure, calculate the expected variation of the heavy fission fragment velocity with mass number for a given initial momentum transfer. The "best fit" lines describing the results of this calculation are shown in Fig. 12. These calculations seem to describe the observations adequately. The deduced value of the fractional linear momentum transfer for the fissioning systems is ~ 0.9 as compared to the value of 0.8 seen for the residue precursors. This distinction between the primary reaction products that fission or de-excite by particle emission is consistent with previous observations for similar reactions.

Having established some confidence that we understand the nature of the fissioning system in these reactions, we can examine the N/Z dependence of the heavy fission fragment yields (Fig. 2). As noted previously, the centroids of the Z distributions are n deficient relative to β stability. The posi-

(a) ^{197}Au + ^{12}C
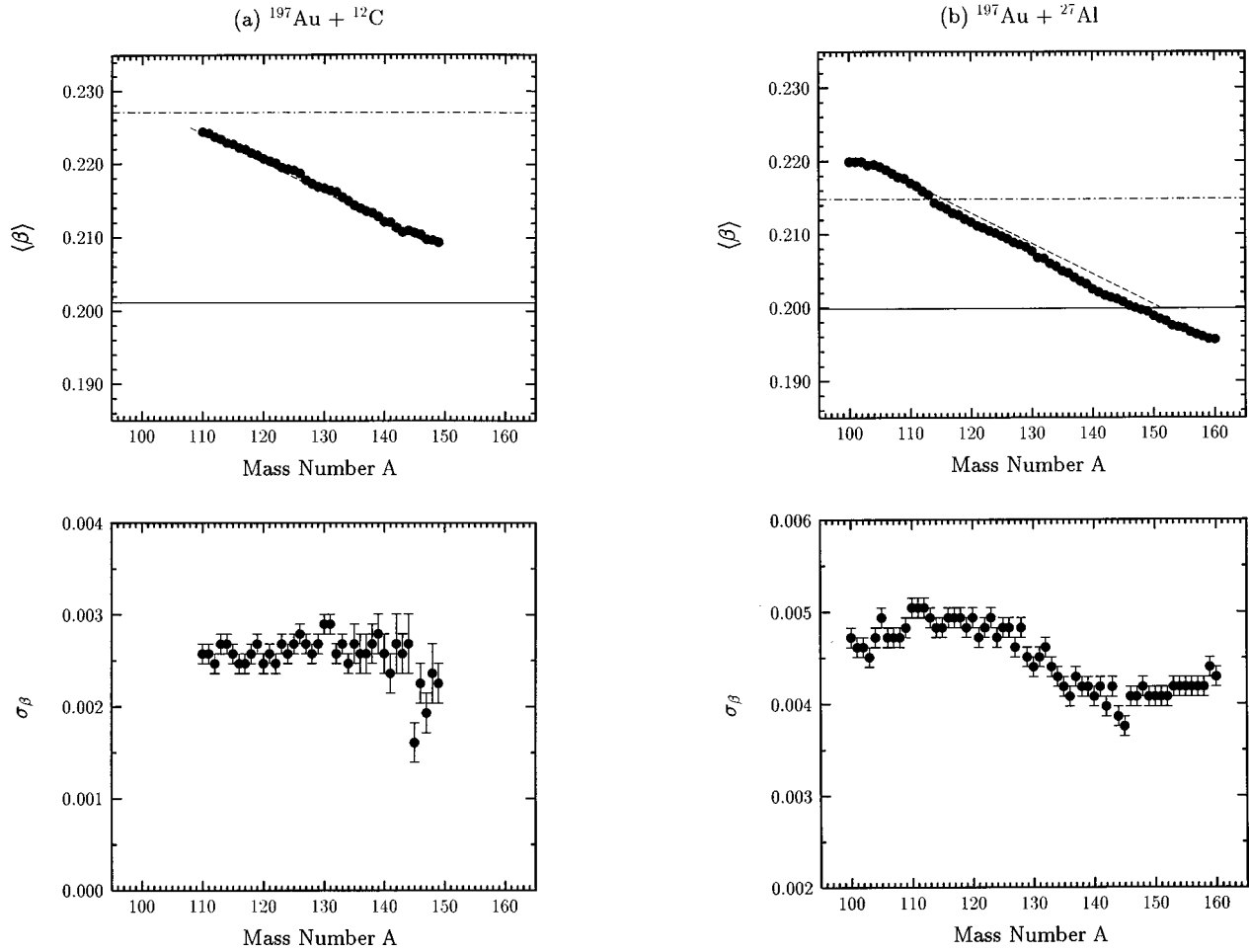
(b) ^{197}Au + ^{27}Al

FIG. 12. Centroid and width of fission fragment velocity distributions as a function of fragment mass for the reaction of 20 MeV/nucleon ^{197}Au with (a) ^{12}C and (b) ^{27}Al. The solid lines in the β vs A distributions represent the expected trend for events involving 90% momentum transfer before fission.

tions of the centroids are in fair agreement with those deduced in a radiochemical study of the same reaction.

An important feature of the fission process is the division of nuclear charge between two fragments. Such charge distributions are frequently parametrized as having a Gaussian form

$$Y(Z) = \frac{1}{(2\pi)^{1/2}\sigma_Z^2} \exp\left[\frac{-(Z-Z_p)^2}{2\sigma_Z^2}\right], \qquad (9)$$

where σ_Z is the Gaussian width parameter and Z_p is the most probable primary fragment atomic number for a given isobaric series. In charge equilibration at fixed mass number, the N/Z mode is commonly described as a harmonic oscillator having a phonon energy $\hbar\omega$ with the charge variance being described as

$$\langle \sigma_Z^2 \rangle = \frac{1}{M\omega^2}\left(\frac{\hbar\omega}{2} + \frac{\hbar\omega}{e^{\hbar\omega/T}-1}\right), \qquad (10)$$

where M is the inertia parameter of the N/Z mode and T is the temperature. At low temperatures typical of thermal neutron induced fission, Eq. (10) becomes

$$\langle \sigma_Z^2 \rangle = \frac{\hbar}{2M\omega}. \qquad (11)$$

Data for thermal neutron-induced fission agree with this prescription [Eq. (11)] and $\langle \sigma_Z^2 \rangle$ can thus be described as a result of the zero point oscillations of a harmonic oscillator in the charge equilibration mode. At higher temperatures, Eq. (10) becomes

$$\langle \sigma_Z^2 \rangle = \frac{T}{M\omega^2}. \qquad (12)$$

In model-independent language, the variance of the fission charge distribution is a function of the isospin correlations in the nuclear ground state and their behavior with increasing temperature.

Very few high-resolution measurements of the fission charge distributions exist at well characterized higher temperatures so that the relationship between the variance for the charge distribution and the nuclear excitation energy [Eq. (12)] has not been characterized experimentally in a satisfactory manner. Radiochemical measurements of the fragment charge distributions are difficult because of the lack of "in-
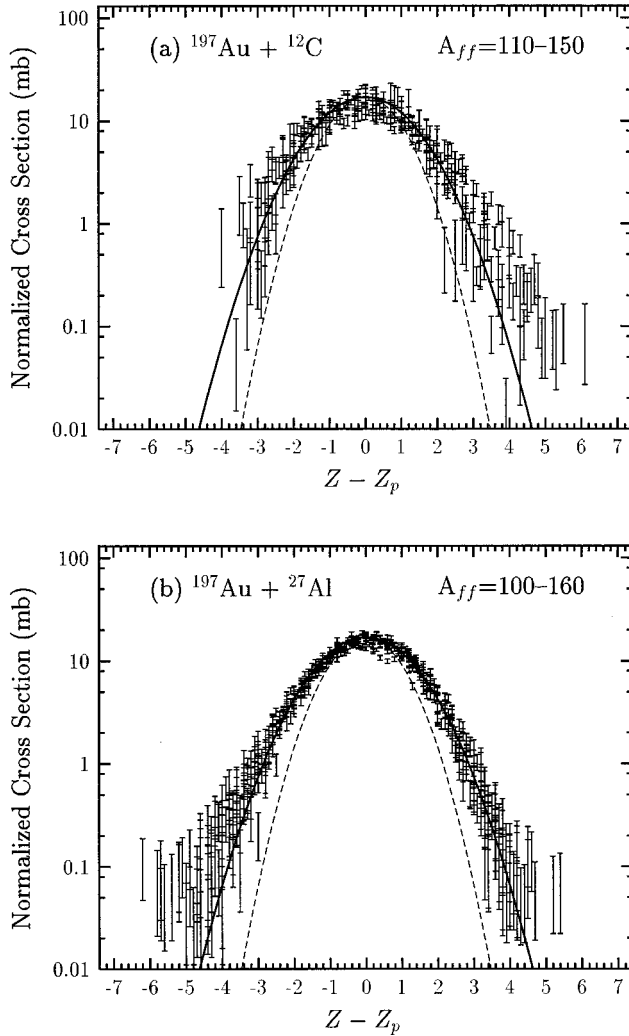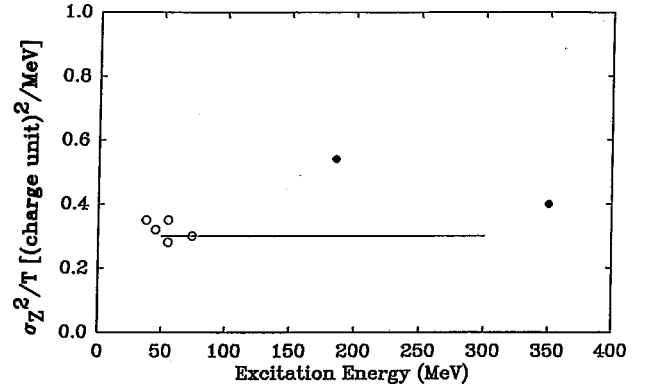
FIG. 14. Values of the fission fragment charge distribution Gaussian width parameter scaled by the temperature of the fissioning system T vs the excitation energy of the fissioning system. The solid circles indicate data from this work while the open circles represent data from low-energy induced fission [27].

$$M\omega^2 = 1.39(A_1^{-1/3} + A_2^{-1/3}) + 186.28\left(\frac{1}{A_1} + \frac{1}{A_2}\right)$$

$$- \frac{2.88}{1.24(A_1^{1/3} + A_2^{1/3})} \tag{14}$$

we can calculate, using Eq. (10), expected values of $\langle\sigma_Z^2\rangle$ for these two systems. The results of that calculation (Fig. 14) indicate the observed variance of the charge distributions exceeds that expected using a model of a time-dependent harmonic oscillator in the charge equilibration mode. Such observations have been made at lower temperatures, but this observation represents one of the first for a well-characterized system at higher temperatures.

IV. RESIDUES FROM FUSIONLIKE COLLISIONS

The ability to isolate and study the properties of the heavy residues from fusionlike collisions offers us the opportunity to test our ability to understand the de-excitation of highly excited heavy nuclei. Because the entrance channel processes should be relatively well understood (and thus the character of the primary product distribution), we can be reasonably sure that we are testing our understanding of the de-excitation processes only when comparing the observations to simulations of the collisions.

The observed secondary product distributions are the result of the initial nuclear encounter, followed by the de-excitation of the primary reaction products by fission or particle emission. To simulate the de-excitation of the primary reaction products, we have used two different computer codes that treat the statistical de-excitation of nuclei, PACE2 [28] and GEMINI [29]. PACE2 is based on the Hauser-Feshbach formalism for the statistical de-excitation of nuclei. It uses Monte Carlo methods to follow the multistep de-excitation. The fission widths are calculated using Bohr-Wheeler expressions for level densities in the fission transition nucleus and rotating liquid drop model barriers. GEMINI uses Monte Carlo techniques and the Hauser-Feshbach formalism to calculate the probabilities of emitting particles with $Z \leq 2$. Heavier fragments and fission fragment emis-

FIG. 13. The fission fragment charge distributions for the studied reactions. The solid line shows the best fit to the data assuming a Gaussian charge distribution. The dashed line shows the expected charge distribution for the thermal model described in the text.

dependent yield'' radionuclides (allowing the measurement of primary fragment yields without intervening β decay).

The present data may offer a unique opportunity to study this problem. The resolution of the A1200 fragment separator, the dominance of fusionlike collisions, and the association of the fissioning nuclei with specific FLMT values allows one to test the harmonic oscillator model or other models of charge equilibration. The fission fragment charge distributions are shown in Fig. 13. As found in the radiochemical studies, all yields can be plotted on a single Gaussian curve with the best fit value of the variance $\langle\sigma_Z^2\rangle$ being 1.2. If we assume that the phonon energy of the deformed fissioning system is given as

$$\hbar\omega \sim \frac{78}{A_1^{1/3} + A_2^{1/3}}(\text{MeV}) \tag{13}$$

and that the stiffness $M\omega^2$ is given as

sion probabilities are calculated using a transition state formalism of Moretto [30].

In addition, GEMINI allows one to simulate the effect of several recent advances in our understanding of the decay of hot, heavy nuclei. One can introduce a fission delay time and its variance, a reduced fission width due to viscous diffusion towards the saddle point (the Kramers factor), the fading of shell corrections with excitation energy, temperature-dependent level density parameters, etc.

For our calculations with PACE2, we have used relatively standard values of the relevant parameters ($a_f/a_n = 1.00$, $a = A/11$) and have not assumed any retardation of fission due to a ''fission delay'' at high excitation energies. However, we did note, using the traceback feature of the code, that for the cases treated, fission occurred relatively late in the evaporation chain ($E^* \sim 135$ MeV) which may be the functional equivalent of a fission delay.

In the GEMINI calculations, we used Lestone's temperature-dependent level density parameter [31], a fading of the shell corrections with excitation energy, enabled IMF emission, and allowed for a retardation of the fission process. For each simulation, we self-consistently varied the fission delay time τ_D and the Kramers width $\Gamma_f^{\text{Kramers}}$ using the relationships [32]

$$\tau_D = \frac{\gamma}{\omega} \ln(10 E_{\text{bar}}/T), \quad (15)$$

$$\frac{\Gamma_f^{\text{Kramers}}}{\Gamma_f^{\text{Bohr-Wheeler}}} = (\sqrt{1+\gamma^2} - \gamma) \quad (16)$$

to give the best fit to the ratio of (fission/residue) formation probability. In these equations the assault frequency ω was taken as $\pi \times 10^{20}$ s.

We have used the ICF model (see Sec. III) to give us the initial primary product distribution to de-excite with both de-excitation codes. The results of these simulations are shown in Fig. 15.

Without any adjustment, the PACE2 simulations gave the approximately correct residue to fission ratio for fusionlike events. [The observed residue survival probabilities were 0.16 (300 mb) for the Au+C reaction and 0.18 (80 mb) for the Au+Al reaction while the simulation predicted 0.18 (330 mb) and 0.14 (60 mb) for the Au+C and Au+Al reactions, respectively.]

For the Au+C reaction, the predicted peak of the mass distribution occurs ~7 mass units below the observed peak and the predicted distribution is much narrower than the measured one. The PACE2 simulations miss the locus of the measured Z_p function by ~0.5 Z units, predicting too n-deficient residues although they do generally reproduce the neutron-deficient character of the observed residues. The predicted yields of the trans-gold nuclei are simply negligible compared to the data. For the Au+Al reaction, there is a better match between the predicted and measured values of the mass distribution peak, although both the predicted width and extent of the distribution is far smaller than observed (although the width of the predicted A distribution for the Al target is substantially larger than that predicted for the C target due to the larger excitation energies in the former sys-
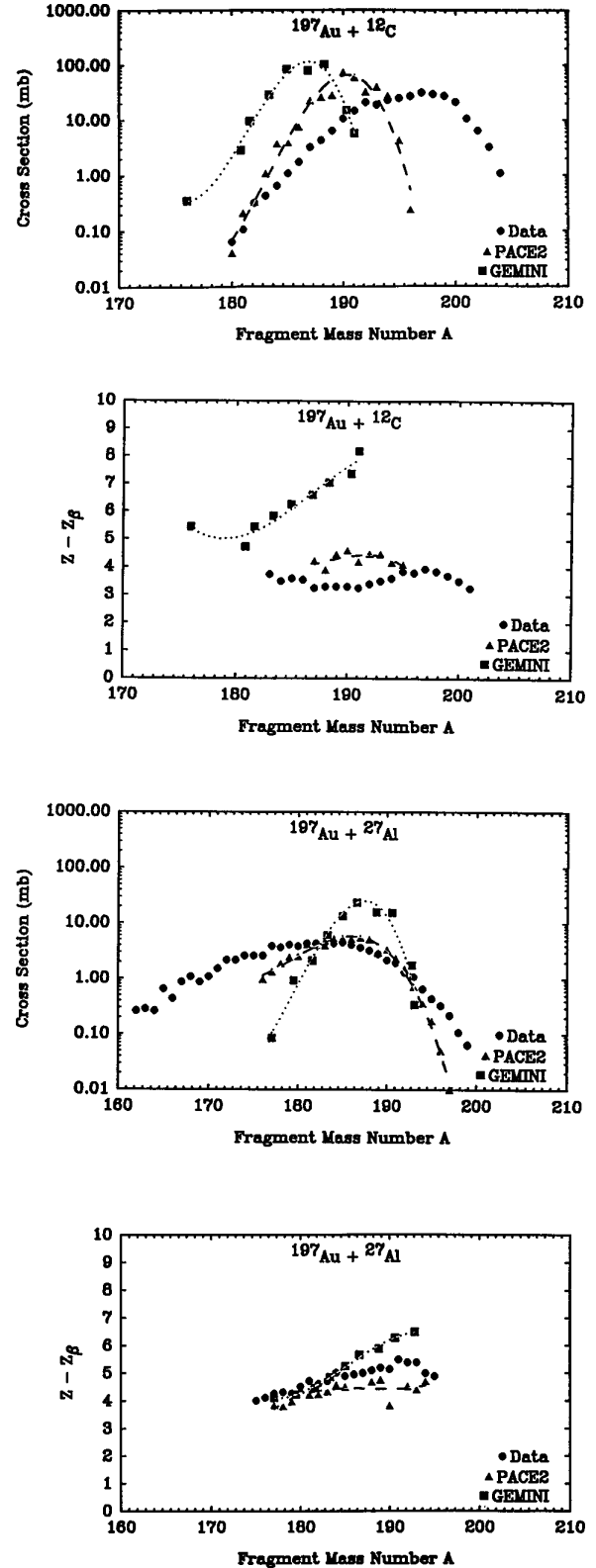

FIG. 15. Comparison of the calculated and measured mass distributions and Z_p functions for the Au+C and Au+Al reactions for fusionlike events.

tem). The failure of a standard statistical model for fusionlike collisions to predict the production of these nuclei has been noted previously [12].

Perhaps it should be noted again *that for fusionlike events* ($v_R/v_{\text{CN}} = 0.7$–0.9), the data show significant yields of

near- and trans-gold products. It is hard to understand how these nuclei are formed. Simply put, each captured projectile nucleon brings in more energy than the energy necessary to remove it and perhaps another nucleon. While the formation of trans-gold products in quasielastic collisions is understandable, their observation in fusionlike collisions can only be due to very unusual de-excitation modes of the primary fragments.

As discussed earlier, in the GEMINI simulations, the fission retardation via the Kramers factor and the fission delay time [Eqs. (15) and (16)] were varied to give a fit to the observed residue survival probability for fusionlike collisions. For the Au+C reaction, the nuclear friction coefficient γ was found to be 35 ($\tau_D = 460 \times 10^{-21}$ s) while for the Au+Al reaction, γ was found to be 20 ($\tau_D = 250 \times 10^{-21}$ s). The lower value of γ for the Au+Al reaction is noted to be 0.57 of γ for the Au+C reaction, which is approximately the ratio of $3.2^2/4.2^2$, the ratio of the inverse squares of the nuclear temperatures of the compound systems. This dependence of γ on $1/T^2$ is consistent with expectations [33] that at some higher temperature ($T \sim$ 2 MeV), the dissipation should go from primarily one-body dissipation (where $\gamma \sim T$ or T^2) to two-body dissipation where $\gamma \sim 1/T^2$.

However reassuring the deduced values of the nuclear friction coefficients are, one sees (Fig. 15) that the GEMINI simulations are not in very good agreement with the observations. The peak in the residue mass distribution is 5–10 A units from the observed peak and the calculated Z_p function is more than 2 Z units more neutron deficient than the observed distribution. It appears that despite the more sophisticated physics base for the GEMINI code, there is no corresponding increased ability to understand the observations of this work.

The failure of standard statistical model calculations to correctly describe the characteristics of the heavy residues from well characterized heavy systems has been seen before. Studies [34] using the SHIP velocity separator to measure the heavy evaporation residues from collisions at 5–15 MeV/nucleon also found significant differences between statistical model predictions (using the code HIVAP) and observations. Fusionlike processes in the reaction of ^{14}N with ^{232}Th at 30 MeV/nucleon [21] were not properly described by a variety of reaction models.

V. CONCLUSIONS

The present study shows there is acceptable agreement between previous radiochemical studies and the present work, although the radiochemical studies are clearly superior for purposes of measuring cross sections as they yield threshold-free, absolute measurements. The principal new finding of this study is the observation of fusionlike events leading to near- and trans-gold species. These observations, while hinted at in previous radiochemical studies [12], are clearly established by the simultaneous observation of the Z, A, and velocity of the residues (a feature not generally available from radiochemical measurements). These heavy, "hard collision" products are not predicted to have significant yields in fusionlike collisions by applicable models for incomplete fusion. Another new finding of some significance is the observation, especially for the Au+Al reaction, of the
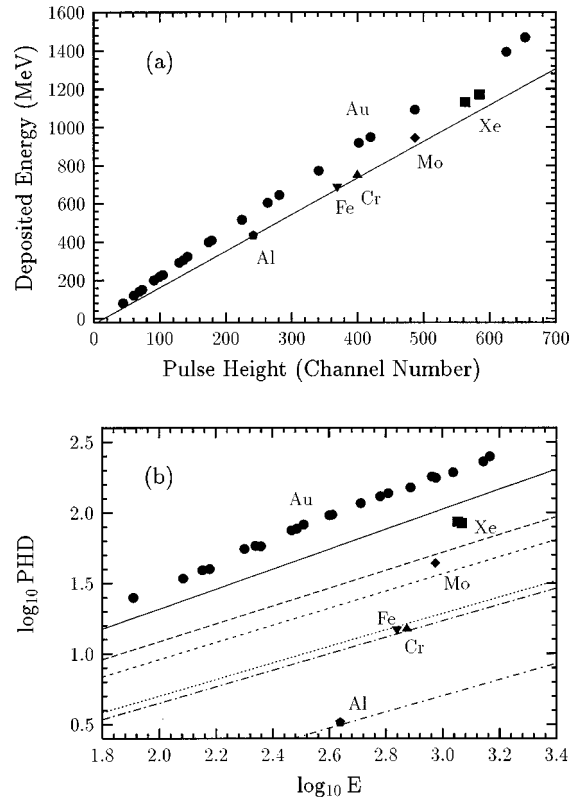

FIG. 16. (a) Deposited energy versus pulse-height correlation for the "stopping" (E) detector. The filled circles indicate the response to Au ions while the other symbols refer to the response to other ions. The straight line represents the detector response to zero-PHD particles (see text). (b) A plot of the pulse-height defect (PHD) vs deposited energy for the stopping detector. The symbols have the same meaning as in (a). The various lines represent the predictions of Moulton's formula.

formation of very neutron-deficient species, possibly involving "unknown" nuclei. The large production cross sections measured in this work suggest a new approach for studying heavy proton-rich nuclei. The fission fragment charge distributions have variances that exceed those expected from models involving a time-dependent harmonic oscillator in the charge equilibration mode. Models of the statistical de-excitation of hot, heavy nuclei seem to describe the overall features of the data for fusionlike collisions, although some discrepancies between the models and between the models and the data exist.

APPENDIX: PULSE HEIGHT DEFECT CORRECTION

In this section, the procedure developed to obtain pulse-height-defect (PHD) corrections for very-heavy ions in the

stopping (E) detector is described. For lack of an appropriate parametrization of PHD at medium energies, we followed the low-energy formalism of Moulton [8]. A plot of deposited energy versus pulse height for this detector is presented in Fig. 16(a). To define the response of the detector to zero-PHD particles we used the measured energy versus pulse-height response of the lighter of the calibration particles (^{27}Al, ^{54}Fe, ^{54}Cr) making zero or small corrections for their PHD using Moulton's formulas. A straight line was fitted to these points and was assumed to represent the detector response curve to zero-PHD particles. PHD's for the heavy-ions were calculated with respect to this calibration line.

The relation of the deduced PHD values to the deposited energy of the calibration ions is presented in a log-log plot in Fig. 16(b). The PHD curves predicted by Moulton's formulas are also displayed for these ions and lie below the PHD values extracted with the present procedure. For example, a ^{197}Au ion depositing 1400 MeV in the detector, has a PHD of 230 MeV according to our procedure, whereas Moulton's formulas give 134 MeV. (Recall that Moulton's formulas are based on measurements of very low-energy heavy ions, whereas energies deposited in the detector in the present measurements are 5–10 times higher.) As seen in Fig. 16(b), the relation of measured PHD versus energy for the ^{197}Au ions is linear (in the log-log plot) with slope approximately equal to that given by Moulton. We thus decided to express the PHD with a simple exponential:

$$\text{PHD} = 10^b E^a, \qquad (A1)$$

where a is the slope and b is the y intercept of the plot of log PHD vs log E. The slope a was taken to be that of Moulton's prescription:

$$a(Z) = 0.02230 \frac{Z^2}{1000} + 0.5682. \qquad (A2)$$

Using these equations and the measured PHD of the calibration ions, values of the intercept b were calculated and fitted, as a function of Z, by the equation

$$b(Z) = 0.473 - 0.2932 \frac{100}{Z} + 0.01332 \left(\frac{100}{Z} \right)^2. \qquad (A3)$$

A PHD analysis was not necessary for the energy-loss calibration of the transmission detectors ($\Delta E_1, \Delta E_2$) for most of the events of interest. (This is consistent with the notion that pulse height defect is an ''end of range'' phenomenon related to the ionization density in the detector.) As already mentioned in Sec. II, a direct correlation of energy loss with pulse height was adequate for the energy-loss reconstruction. However, this was not true for the response of the second transmission detector (ΔE_2) to the slowest particles observed ($E/A \approx 14$ MeV) which were almost stopping in this detector. For these events, a PHD correction procedure similar to the one described for the E detector was applied in which, the parameter b was expressed as a function of the fractional velocity change through this detector.

---

[1] K. Aleklett, M. Johansson, L. Sihver, W. Loveland, H. Groening, P. L. McGaughey, and G. T. Seaborg, Nucl. Phys. **A149**, 591 (1989).

[2] W. Loveland, K. Aleklett, L. Sihver, Z. Xu, C. Casey, D. J. Morrissey, J. O. Liljenzin, M. de Saint-Simon, and G. T. Seaborg, Phys. Rev. C **41**, 973 (1990).

[3] D. Bazin, D. Guerreau, R. Anne, D. Guillemand-Mueller, A. C. Mueller, and M. G. Saint-Laurent, Nucl. Phys. **A515**, 349 (1990).

[4] B. Faure-Ramstein, F. Auger, J. P. Wieleczko, W. Mittig, A. Cunsolo, A. Foti, E. Plagnol, J. Quebert, and J. M. Pascaud, Nucl. Phys. **A586**, 533 (1995).

[5] K. A. Hanold *et al.*, Phys. Rev. C **52**, 1462 (1995).

[6] F. Hubert, R. Bimbot, and H. Gauvin, At. Data Nucl. Data Tables **46**, 1 (1990); Nucl. Instrum. Methods Phys. Res. B **36**, 357 (1989).

[7] B. M. Sherrill, D. J. Morrissey, J. A. Nolen, and J. A. Winger, Nucl. Instrum. Methods Phys. Res. B **56/57**, 1106 (1991).

[8] J. B. Moulton, J. E. Stephenson, R. P. Schmitt, and G. J. Wozniak, Nucl. Instrum. Methods **157**, 325 (1978).

[9] E. Baron, M. Bajard, and Ch. Ricaud, Nucl. Instrum. Methods Phys. Res. A **328**, 177 (1993).

[10] G. A. Souliotis *et al.*, Nuclear Chemistry Progress report, 1995, Oregon State University, pp. 27–32.

[11] B. M. Sherrill (private communication).

[12] H. Kudo, K. J. Moody, and G. T. Seaborg, Phys. Rev. C **30**, 1561 (1984).

[13] G. Friedlander, J. W. Kennedy, E. S. Macias, and J. M. Miller, *Nuclear and Radiochemistry*, 3rd ed. (Wiley, New York, 1981), p. 45.

[14] E. Piasecki *et al.*, Phys. Lett. B **351**, 412 (1995).

[15] P. L. McGaughey, W. Loveland, D. J. Morrissey, K. Aleklett, and G. T. Seaborg, Phys. Rev. C **31**, 896 (1985).

[16] K. Sümmerer, W. Brüchle, D. J. Morrissey, M. Schadel, B. Szweryn, and Yang Weifan, Phys. Rev. C **42**, 2546 (1990).

[17] C. Gregoire and B. Tamain, Ann. Phys. (Paris) **11**, 323 (1986).

[18] F. P. Hessberger, V. Ninov, S. Hofmann, D. Ackerman, S. Saro, and M. Veselsky, Z. Phys. A **348**, 301 (1994).

[19] H. M. Blann, Phys. Rev. C **23**, 205 (1981).

[20] A. A. Sonzogni *et al.*, Phys. Rev. C **53**, 243 (1996).

[21] H. W. Leegte, A. L. Boonstra, J. D. Hinnefeld, E. E. Koldenhof, R. H. Siemssen, K. Siwek-Wilczynska, Z. Sosin, J. Wilczynski, and H. W. Wilschut, Phys. Rev. C **46**, 991 (1992).

[22] J. L. Wile *et al.*, Phys. Rev. C **45**, 2300 (1992).

[23] D. Jouan *et al.*, Z. Phys. A **340**, 63 (1991).

[24] M. B. Tsang, G. F. Bertsch, W. G. Lynch, and M. Tohyama, Phys. Rev. C **40**, 1685 (1989).

[25] D. J. Parker, P. Vergani, E. Gladioli, J. J. Hogan, F. Vettore, E. Gladioli-Erba, E. Fabrici, and M. Galmarini, Phys. Rev. C **44**, 1528 (1991).

[26] C. N. Davids *et al.*, Phys. Rev. Lett. **76**, 592 (1996).

[27] Y. T. Oganessian and Y. A. Lazarev, in *Treatise in Heavy Ion Science*, edited by D. A. Bromley (Plenum, New York, 1985), Vol. 4, pp. 3–251.

[28] A. Gavron, in *Computational Nuclear Physics 2*, edited by K. Langanke, J. A. Maruhn, and S. E. Koonin (Springer-Verlag, New York, 1993), pp. 108–114.

[29] R. Charity *et al.*, Nucl. Phys. **A483**, 391 (1988).

[30] L. G. Moretto, Nucl. Phys. **A247**, 211 (1975).

[31] J. P. Lestone, Phys. Rev. C **52**, 118 (1995).

[32] P. Paul and M. Thoennessen, Annu. Rev. Nucl. Part. Sci. **44**, 70 (1994).

[33] B. W. Bush, G. F. Bertsch, and B. A. Brown, Phys. Rev. C **45**, 1709 (1992); see also, D. J. Hofman, B. B. Back, and P. Paul, *ibid.* **51**, 2597 (1995).

[34] F. P. Hessberger, V. Ninov, D. Ackermann, and A. Lùttgen, Nucl. Phys. **A568**, 121 (1994); F. P. Hessberger, V. Ninov, and U. Spoerel, Z. Phys. A **340**, 171 (1991).